

# 1 The influence of glacial landscape evolution on Scandinavian 2 Ice Sheet dynamics and dimensions

3 Gustav Jungdal-Olesen <sup>1</sup>, ~~Vivi Kathrine Pedersen<sup>†</sup>~~, Jane Lund Andersen<sup>2</sup>, Andreas Born<sup>3</sup>, Vivi Kathrine  
4 Pedersen<sup>1</sup>

5 1) Department of Geoscience, Aarhus University, Aarhus, Denmark

6 2) Department of Physical geography, Stockholm University, Stockholm, Sweden

7 3) Department of Earth Science and Bjerknes Centre for Climate Research, University of Bergen, Bergen,  
8 Norway

9 *Correspondence to:* Gustav Jungdal-Olesen ([gpo@geo.au.dk](mailto:gpo@geo.au.dk))

10 NOTE: Figures in this document with track changes are the old unrevised figures. Having multiple versions of figures in  
11 the document makes it very unstable and makes Microsoft Word crash on my computer. The complete manuscript file  
12 without track changes includes the revised figures, which can be seen at the end of the manuscript.

## 13 Abstract

14 The Scandinavian topography and bathymetry have been shaped by ice through numerous glacial cycles in the  
15 Quaternary. In this study, we investigate how the changing morphology has influenced the Scandinavian ice  
16 sheet (SIS) in return. We use a higher-order ice-sheet model to simulate the SIS through a glacial period on  
17 three different topographies, representing different stages of glacial landscape evolution in the Quaternary. By  
18 forcing the three experiments with the same climate conditions, we isolate the effects of a changing landscape  
19 morphology on the evolution and dynamics of the ice sheet. We find that early Quaternary glaciations in  
20 Scandinavia were limited in extent and volume by the pre-glacial bathymetry until glacial deposits filled  
21 depressions in the North Sea and build out the Norwegian shelf. From middle/late Quaternary (~0.5 Ma) the  
22 bathymetry was sufficiently filled to allow for a faster southward expansion of the ice sheet causing a relative  
23 increase in ice-sheet volume and extent. Furthermore, we show that the formation of The Norwegian Channel  
24 during recent glacial periods restricted southward ice-sheet expansion, only allowing for the ice sheet to  
25 advance into the southern North Sea close to glacial maxima. Finally, our experiments indicate that different  
26 stretches of The Norwegian Channel may have formed in distinct stages during glacial periods since ~0.5 Ma.  
27 These results highlight the importance of accounting for changes in landscape morphology through time when  
28 inferring ice-sheet history from ice-volume proxies and when interpreting climate variability from past ice-  
29 sheet extents.

## 30 31 1 Introduction

32 Ice holds the power to transform landscapes and constituted a major geomorphological agent in northern  
33 Europe during the Quaternary (last 2.6 Ma) where recurring glacial cycles shaped the present-day landscape.  
34 Indeed, the topography and bathymetry in and around northern Europe reveal the extensive impact of its rich  
35 glacial history, with deep fjords and U-shaped valleys attesting to the accumulated effect of widespread glacial  
36 erosion and terminal moraines indicating the extent of past ice sheets (~~Hughes-Hughes et al., 2016; Stroeven~~

37 at al., 2016). The Eurasian ice sheet complex covered much of the British Isles, all of Scandinavia, and much  
38 of northern Europe including parts of Germany, Poland, Russia, and the Baltic through multiple glacial cycles  
39 since 1 Ma (Batchelor et al., 2019). During the Last Glacial Maximum (LGM), the complex consisting of the  
40 Scandinavian ice sheet (SIS), the Barents Sea ice sheet (BSIS), and the British-Irish ice sheet (BIIS), contained  
41 an ice volume corresponding to  $\sim 18.4 \pm 4.9$  m sea-level equivalent (Simms et al., 2019). On a global scale, the  
42 pace of these glacial cycles results from solar insolation variations combined with feedback mechanisms and  
43 internal dynamic effects in the climate system, in part caused by the ice sheets themselves (Hughes and  
44 Gibbard, 2018). Differences in ice volume and extent of ice sheets between glacial cycles (Fig. 1) can also be  
45 attributed to variations in moisture supply through complex global atmosphere-ocean-ice interactions (e.g.,  
46 Batchelor et al., 2019; Hughes and Gibbard, 2018), with topography and proximity to the ocean being key  
47 factors determining the spatial distribution of moisture to an ice sheet. Studies on glacial landscape evolution  
48 have indicated that glacial erosion and deposition can also influence ice-sheet dynamics, ice volumes, and  
49 extent (e.g., Kessler et al., 2008; Kaplan et al., 2009; MacGregor et al., 2009; Egholm et al., 2009, 2012a,b,  
50 2017; Anderson et al., 2012; Pedersen and Egholm, 2013; Pedersen et al., 2014; Claque et al., 2020; Mas e  
51 Braga et al., 2023). But until now, these studies have been limited to synthetic landscapes and/or limited spatial  
52 scales (smaller glaciers and ice caps). A few ice-sheet scale models are starting to consider glacial erosion  
53 (e.g., Patton et al., 2022), but the effects of long-term Quaternary landscape evolution on ice-sheet dynamics  
54 are still to be explored on a large scale for realistic landscapes and ice-sheet configurations. Understanding



55 the influence of landscape evolution on ice-sheet dynamics requires the reconstruction of landscapes that  
56 existed prior to or at earlier stages of glacial erosion, something that can be approached using source-to-sink  
57 studies, utilizing off-shore sediment volumes of a glacial origin (e.g., Steer et al., 2012; Paxman et al. 2019;  
58 Pedersen et al., 2021).

59



60  
61  
62  
63  
64  
65  
66  
67  
68  
69  
70  
71  
72  
73  
74  
75  
76  
77  
78  
79  
80  
81  
82  
83  
84  
85  
86  
87  
88  
89  
90  
91  
92  
93  
94  
95  
96  
97

*FIG. 1. Overview map of model domain. Maximum plausible extent of the Fennoscandian ice sheet complex during last glacial maximum (LGM, black line) and penultimate glacial maximum (MIS6, red dashed line) are overlaid (Batchelor et al., 2019) as well as the approximate location of the LGM ice divide position (Olsen et al., 2013).*

In this work, we focus on the well-studied Scandinavian region and investigate how the SIS may have changed its behaviour because of Quaternary landscape evolution. We use a higher-order ice-sheet model to investigate how large-scale glacial morphological features have influenced the development and dynamics of the SIS over a glacial cycle at two key times during the Quaternary: 1) before the inception of major glaciations in the beginning of the Quaternary (PREQ ~2.6 Ma) and 2) during the middle/late Quaternary (MLQ ~0.5 Ma) where major pre-glacial features in the bathymetry around Scandinavia had been filled with glacial deposits (Dowdeswell and Ottesen, 2013). Importantly, we do not intend to reconstruct realistic SIS configurations for these past time periods, but rather keep the climate forcing consistent between experiments, in order to isolate how changes in bed morphology has impacted SIS dynamics and extent. This allows us to i) explore how morphological changes can influence the dynamics, extent, and volume of the ice sheet, independent of the climatic forcing, and ii) gain insight into how ice-volume proxies could be influenced by glacial landscape evolution.

For the early Quaternary, we adopt the pre-glacial landscape reconstructions provided for the Scandinavian region by Pedersen et al. (2021) that include i) ~~removal-the absence~~ of glacially generated sediments offshore, ii) ~~infilling~~ of over-deepened fjords and glacial valleys onshore, iii) ~~reconstruction-of-a~~ reconstructed wedge of older Mesozoic and Cenozoic sediments on the inner shelf that is assumed to have been eroded by glacial activity within the Quaternary (e.g., Hall et al., 2013), and finally, iv) adjustments of the landscape owing to erosion- and deposition-driven isostatic changes and dynamic topography (Pedersen et al., 2016).

In addition to this pre-glacial reconstruction, that explores an entirely different offshore bathymetry and onshore Scandinavian landscape, we also consider the more subtle effects of the large glacial troughs that have been carved into the shelf bathymetry by ice streams since the middle/late Quaternary. One of the most notable of these glacio-morphological features offshore Scandinavia is ~~T~~the Norwegian Channel (Fig. 1). This channel is believed to have been formed by ice-stream activity sometime since 1.1 Ma (e.g., Sejrup et al. 2003), with studies suggesting that ~90 % of the deposits funneled through the channel and into the North Sea Fan were deposited within the last ~0.5 Ma (Hjelstuen et al., 2012). Recently, ~~its~~ has been ~~argued~~suggested that the channel formed ~~mostly within the last~~before ~0.35 Ma (Løseth et al., 2022). An erosional unconformity at the base of the channel is draped by post-LGM sediments, suggesting that the channel experienced erosion within the last glacial cycle (Hjelstuen et al., 2012). ~~For the last glacial cycle, it has been proposed that the Norwegian Channel Ice Stream (NCIS) was active in stages but mainly during the LGM (e.g., Sejrup et al., 1998; Sejrup et al., 2003). Ice streaming in the outer parts of the channel near the shelf break started close to the LGM with~~

98 ~~increased activity promoting ice retreat around 19 ka BP because of the increased ice mass loss (Sejrup et al.,~~  
99 ~~2016). The retreat translated southwards over time as the SIS unzipped from the adjacent BHS after which~~  
100 ~~with ice streaming was mostly confined to the main trunk of the channel (Sejrup et al., 2016).-~~

## 102 2 Methods

103 For the numerical experiments presented in this study, we use the depth-integrated second-order shallow-ice  
104 approximation iSOSIA (Egholm et al., 2011, 2012a,b). We conduct our experiments by simulating a full glacial  
105 cycle of 120 ka on different topographies. In the following section we will present the numerical model, the  
106 model setup, and the experimental design.

### 108 2.1 Modelling the Scandinavian Ice Sheet

109 The ice flow in iSOSIA is governed by a second-order approximation of the equations for Stokes flow (e.g.,  
110 Egholm et al., 2011). The velocities are depth integrated to yield a 2D one layer ice model, implemented here  
111 using a regular grid (e.g., Egholm and Nielsen, 2010). The second-order nature of the approximation ensures  
112 that ice velocities depend non-linearly on ice thickness, ice-surface gradients, as well as longitudinal and  
113 transversal horizontal stress gradients (Egholm et al., 2011, 2012b). Details on the iSOSIA model, including  
114 the importance of the higher order ice dynamics involved, have been described in depth elsewhere (Egholm  
115 and Nielsen, 2010; Egholm et al., 2011, 2012a,b).

117 The depth-integrated ice-creep velocity is calculated using temperature-dependent Glen's flow with a stress  
118 exponent,  $n$ , equal to 3:

$$120 \dot{\epsilon}_{ij} \epsilon_{ij} = A_{flow} \tau_e^{n-1} s_{ij},$$

122 where  $\dot{\epsilon}\epsilon$  is the strain rate tensor,  $ij$  denoting the components of the tensor,  $A_{flow}$  is the ice flow parameter,  $\tau_e$   
123 is the effective stress and  $s$  is the deviatoric stress tensor (Egholm et al., 2011). The ice flow parameter  $A_{flow}$   
124 is dependent on the depth averaged temperature of the ice using an exponential relationship:

$$125 A_{flow} = A_0 \exp\left(\frac{-Q}{RT}\right),$$

126 where  $A_0$  is a flow constant,  $Q$  is an activation energy,  $R$  is the gas constant and  $T$  is the temperature relative  
127 to the pressure melting point (e.g., Zeitz et al. 2020).  $A_0$  and  $Q$  have different values above and below  $T = -10$   
128  $^{\circ}\text{C}$  (see table 1).-A simple Weertman sliding scheme is used to calculate the contribution of basal sliding to  
129 depth-integrated ice velocities:

$$130 u_b = A_{sliding} \frac{t_s^3}{N},$$

132 where  $u_b$  is the basal velocity,  $A_{sliding}$  is an ice sliding coefficient,  $t_s$  is the bed parallel shear stress and  $N$   
133 is the effective pressure at the base (Egholm et al. 2011).  $A_{sliding}$  is chosen to give realistic sliding in the order  
134 of several hundred meters per year for example in fjords or near the shelf edge in the Norwegian Sea, similar

135 to surface velocities in comparable areas of modern-day ice-bodies (e.g., Millan et al. 2022) . To allow for  
 136 faster ice flow for soft bed subglacial conditions (e.g., Gladstone et al., 2020, Han et al., 2021),  $A_{sliding}$  is  
 137 enhanced by a factor of 5 in offshore regions and onshore in northern Europe where thick, soft sediments cover  
 138 the bed.

139  
 140  
 141  
 142 In this study, we focus on grounded ice only, as ice-shelf dynamics are computationally expensive to resolve  
 143 on the timescales of our experiment and because constraints on ice shelf extent in middle or early Quaternary  
 144 glaciations are sparse due to a lack of reliable dates on submarine landforms (e.g., Jakobsson et al. 2016).  
 145 Some older studies suggest that an ice shelf was present during recent glaciations in the North Atlantic and  
 146 Arctic regions (Hughes et al. 1977, Lindstrom et al. 1986). However, while ice shelf stability is sensitive to  
 147 bathymetric configurations (Bart et al. 2016) and is a deciding factor in grounding line migration, we limit our  
 148 focus here to large-scale morphological features, such as the Norwegian Channel, created by an ice stream in  
 149 contact with the sea-bed (Sejrup et al., 2016). Consequently, we do not consider floating ice in our simulations  
 150 and remove floating ice by introducing a fast melt rate for ice that does not meet the grounding criterion:

$$151 \quad H_{ice} > (SL + H_{ice}) \frac{\rho_{water}}{\rho_{ice}},$$

152 where  $H_{ice}$  is ice thickness, SL is local sea level and  $\rho_{water}$  and  $\rho_{ice}$  are the densities of water and ice, respectively.

153 Mean sea level in the model is varied between interglacial and glacial maximum (-130 m) using the normalized  
 154 LR04 Benthic Stack (Lisiecki and Raymo, 2005) as a glacial index. Special boundary conditions are employed  
 155 at the approximate locations where the SIS meets the BSIS and BISS by introducing an ‘ice wall’ where the  
 156 ice flux is zero to emulate divergent ice flow when these ice sheets merge during glacial maxima. At the edges  
 157 of the model domain, we employ open boundary conditions to allow for ice to flow out of the domain. Common  
 158 model parameters are presented in Table 1.

159

Parameter		Value	Unit
$\rho_{ice}$	Ice density	910	kg m <sup>-3</sup>
$q_b$	Geothermal heat flux	0.045	W m <sup>-2</sup>
$L_i$	Latent heat of ice	334	kJ kg <sup>-1</sup>
$A_{flow}$	Ice flow parameter	$1.5 \cdot 10^{15}$	Pa <sup>-2</sup> y <sup>-1</sup>
$A_{sliding}$	Ice sliding parameter	0.4	m Pa <sup>-2</sup> y <sup>-1</sup>
$n$	Ice flow exponent	3	
$f_{flow\ enhancement}$	Ice flow enhancement factor	100	
$m$	Ice sliding exponent	3	
$F_{sliding\ enhancement}$	Sliding enhancement factor offshore	5	
$mPDD$	PDD factor	0.005	m °C <sup>-1</sup> d <sup>-1</sup>

$SL$	Mean sea level	$[0 : 130]$	m
$dT_h$	Lapse rate	6.5	$^{\circ}\text{C km}^{-1}$
$dT_{m,e}$	Easterly temperature gradient	$[-1.3 : 2.3] \cdot 10^{-6}$	$^{\circ}\text{C m}^{-1}$
$dT_{m,n}$	Northerly temperature gradient	$[-3.5 : -10] \cdot 10^{-6}$	$^{\circ}\text{C m}^{-1}$
$dA_{T,e}$	Easterly annual temperature variation gradient	$[7.8 : 0.11] \cdot 10^{-6}$	$^{\circ}\text{C m}^{-1}$
$dA_{T,n}$	Northerly annual temperature variation gradient	$[2.0 : 1.4] \cdot 10^{-6}$	$^{\circ}\text{C m}^{-1}$
$dP/dT$	Change in precipitation with change in temperature	0.029	$^{\circ}\text{C}^{-1}$
$D_L$	Thickness of elastic lithosphere	50	km

160

<u>Parameter</u>	<u>Parameter description</u>	<u>Value</u>	<u>Unit</u>
$A_{\text{flow}}$	Ice flow parameter	$[3.615 \cdot 10^{-13} : 1.733 \cdot 10^3]$	$\text{s}^{-1} \text{Pa}^{-3}$
$A_{\text{sliding}}$	Ice sliding parameter	0.4	$\text{m Pa}^{-2} \text{y}^{-1}$
$dA_{T,e}$	Easterly annual temperature variation gradient	$[0.11 : 7.8] \cdot 10^{-6}$	$^{\circ}\text{C m}^{-1}$
$dA_{T,n}$	Northerly annual temperature variation gradient	$[1.4 : 2.0] \cdot 10^{-6}$	$^{\circ}\text{C m}^{-1}$
$D_L$	Thickness of elastic lithosphere	50	km
$dP/dT$	Change in precipitation with change in temperature	0.029	$^{\circ}\text{C}^{-1}$
$dT_h$	Lapse rate	6.5	$^{\circ}\text{C km}^{-1}$
$dT_{m,e}$	Easterly temperature gradient	$[-1.3 : -2.3] \cdot 10^{-6}$	$^{\circ}\text{C m}^{-1}$
$dT_{m,n}$	Northerly temperature gradient	$[-3.5 : -10] \cdot 10^{-6}$	$^{\circ}\text{C m}^{-1}$
$f_{\text{flow enhancement}}$	Ice flow enhancement factor	100	-
$E_{\text{sliding enhancement}}$	Sliding enhancement factor offshore	5	-
$L_i$	Latent heat of ice	334	$\text{kJ kg}^{-1}$
$m$	Ice sliding exponent	3	-
$m\text{PDD}$	PDD factor	0.005	$\text{m } ^{\circ}\text{C}^{-1} \text{d}^{-1}$
$n$	Ice flow exponent	3	-
$Q$	Activation energy for calculating $A_{\text{flow}}$	$[6.0 : 13.9] \cdot 10^4$	$\text{J mol}^{-1}$
$q_b$	Geothermal heat flux	0.045	$\text{W m}^{-2}$
$SL$	Mean sea level	$[-130 : 0]$	m
$\rho_{\text{ice}}$	Ice density	910	$\text{kg m}^{-3}$

161

162

163 **TABLE 1.** Common parameters in the ice sheet model and mass balance scheme. Numbers in brackets  
164 denote min and max values.

165

### 166 2.1.1 Mass balance

167 In the simulations we present here, we assume that the mass balance ( $\dot{M}_{ice}$ ) of the ice sheet can be  
168 approximated using three components:

169

$$\dot{M}_{ice} = \dot{m}_{acc} - \dot{m}_s - \dot{m}_b,$$

170 where  $\dot{m}_{acc}$  is the rate of accumulation,  $\dot{m}_s$  is the surface melt rate and  $\dot{m}_b$  is the basal melt rate (Egholm et  
171 al. 2012b). We use a positive-degree-day (PDD) model to estimate accumulation rate and surface melt rate as

172 a function of mean annual temperature, annual temperature variation, and mean annual precipitation at every  
173 point in our model domain for every time step (e.g., Magrani et al., 2022).

174 The yearly temperature variation in a given cell, is approximated by a sine function based on the mean annual  
175 temperature and annual temperature amplitude (see below). The melt rate in m/yr is calculated in the PDD  
176 model as:

$$177 \quad \dot{m}_s = m_{PDD} \sum_{n=1}^{365} T_{positive},$$

178 where  $m_{PDD}$  is the positive-degree-day factor multiplied with the sum of positive degrees ~~each year~~  $T_{positive}$  ~~each~~  
179 ~~year~~. Here, we consider a single melting degree factor for both ice and snow, since all precipitation is turned  
180 into ice after accumulation (based on yearly average rates). The accumulation rate is approximated by:

181

$$182 \quad \dot{m}_{acc} = \frac{n_{frost}}{365} \cdot P,$$

183 where  $n_{frost}$  is the number of days with negative temperatures in a year and  $P$  is the annual precipitation. The  
184 temperature forcing that drives spatial and temporal changes in mass balance in our simulations is based on  
185 mean temperature, annual temperature amplitude, and lapse rate that vary across the model domain using  
186 spatial gradients that vary in time. Two climate states are chosen to represent the extremes of our model: a  
187 glacial maximum state and an interglacial state, and the spatial gradients of the full glacial cycle of our model  
188 simulations are subsequently defined to vary in between these extremes using a glacial index that resembles  
189 the normalized LR04 Benthic Stack (Lisiecki and Raymo, 2005) with glacial maximum in this climate forcing  
190 occurring at 18 ka BP. Here we define spatial ( $x, y, z$ ) gradients at the glacial maximum using multiple linear  
191 regression on MPI-ESM climate model outputs (LGM experiment; Jungclauss et al. 2019). For the interglacial  
192 state we define spatial gradients using the ERA-interim reanalysis data for modern day (Dee et al. 2022).  
193 Finally, the lapse rate was found to be close to constant, so we keep this fixed at  $6.5 \text{ }^\circ\text{C km}^{-1}$ . With this  
194 approach, the temporally ~~varying~~ temperature forcing of the entire grid can be defined from a single grid cell  
195 in the lower left corner ~~and while~~ still capturing a coastal-continental (east-west) gradient, a polar gradient  
196 (south-north), and an altitudinal gradient (lapse rate) in temperature. However, we cannot capture local effects  
197 that arise from changes in complex atmospheric circulations patterns over time that might have important  
198 implications for glacial dynamics and ice extent (e.g., Liakka et al. 2016, Hughes and Gibbard, 2018).

199

200 To represent precipitation in our simulations, we use a climate-corrected modern-day mean precipitation field  
201 (Pendergrass et al., 2022), modulating the local precipitation in every grid cell using the following equation:

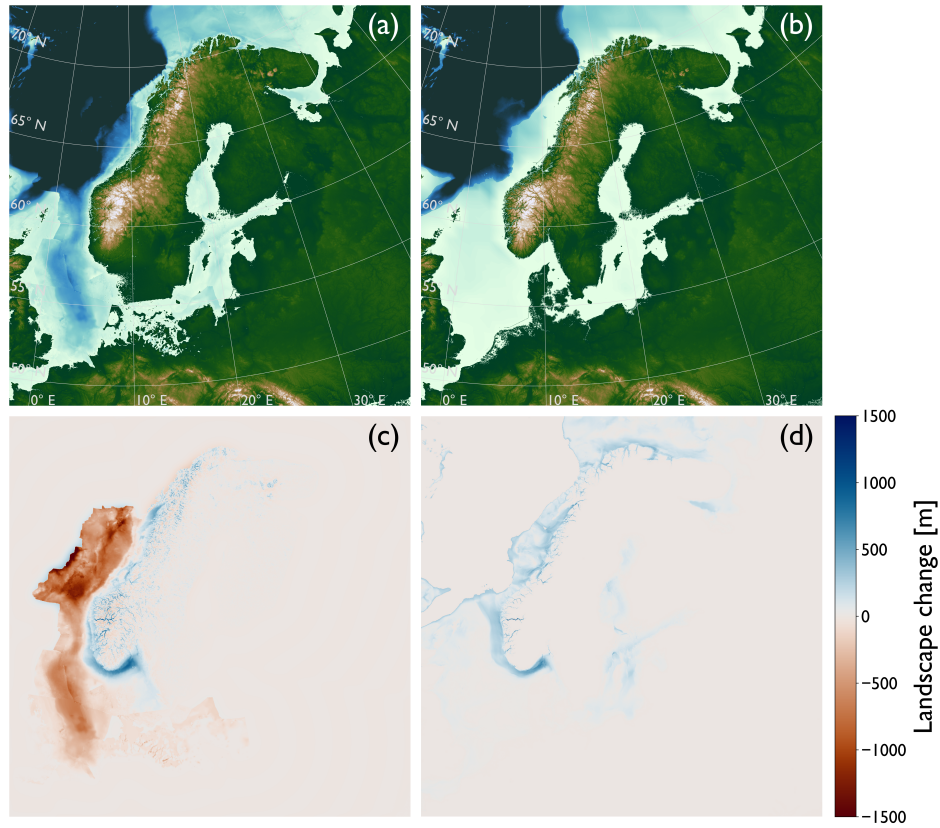
$$202 \quad P = P_0 \cdot e^{kTp \cdot \Delta T},$$

203 where  $P_0$  is the local modern day (interglacial) precipitation,  $\Delta T$  is the change in temperature in a cell from the  
204 previous time step, and  $kTp$  represents the rate of change in precipitation for a change in temperature with a  
205 value of  $0.029 \text{ }^\circ\text{C}^{-1}$ . The value of  $kTp$  is found by optimization through a comparison between mean  
206 precipitation at LGM in MPI-ESM and mean precipitation in the modern-day ERA-interim data set. By scaling  
207 the precipitation with changes in temperature we can capture some of the effects an ice sheet will impose on  
208 moisture supply, by limiting snow-fall in the central parts of the ice sheet (Fig. 3D).



209

210 Basal melting rate is calculated as the difference between  $q_b$  geothermal heat flux from the bed and the heat  
211 flux from the temperature gradient in the basal ice  $q_c$  (Egholm et al., 2012a):



212

213

$$\dot{m}_b = \frac{q_b - q_c}{\rho_{ice} L_i}$$

214 where  $L_i$  is the latent heat for fusion of ice and  $\rho_{ice}$  is the density of ice (Tab. 1).

215

216 **FIG. 2. Paleo-topographic and bathymetric reconstructions. a) the PREQ experiment, b) the MLQ**  
217 **experiment, c) and d) show the differences between the panel above and the modern-day topography and**  
218 **bathymetry.**

219

220

221

### 222 2.1.2 Topography and bathymetry

223 The focus of this study is to examine the influence of bed topography on ice sheet behaviour, exemplified by  
224 simulating the SIS on landscape configurations representing different periods in the Quaternary. For  
225 comparison, we simulate the SIS on modern-day topography and bathymetry over the last glacial cycle in a  
226 reference model. The reference experiment uses the global DEM GEBCO 2022 [grid](#) (GEBCO Bathymetric  
227 Compilation Group., 2022) [global grid](#) sampled at 10 km x 10 km for the ice model (the same grid resolution  
228 is used in all experiments). Because of computational limitations, a model resolution higher than 10 km is not

229 feasible. Having a higher resolution would allow us to resolve glacial morphology in higher detail and could  
230 lead to interesting findings regarding the influence of fjord systems in western Norway on ice sheet dynamics.  
231 Here, we focus on larger features such as the Norwegian Channel where a 10 km resolution is sufficient.  
232 Throughout the model simulations, ice-driven isostasy is handled with a two-dimensional uniform thin elastic  
233 plate model (e.g., Pedersen et al. 2014).

234

235 The pre-glacial landscape is adopted from Pedersen et al. (2021) and reconstructed using a source-to-sink  
236 approach that also considers i) a component of glacial erosion that has taken place on the inner shelf, ii)  
237 erosion-driven isostasy, and iii) a component of dynamic topography (Pedersen et al., 2016). For further details  
238 on the approach see Pedersen et al. (2021). Here, we extend these previous reconstructions and remove the  
239 Quaternary sediment package from all sectors of the North Sea, to reconstruct a realistic pre-glacial bathymetry  
240 for the entire region (Binzer et al., 1994; Rise et al., 2005; Nielsen et al., 2008; Gołędowski et al., 2012; Lamb  
241 et al. 2018; The Southern Permian Basin Atlas). These additional sediment volumes, from outside of the  
242 Norwegian and Danish sectors, are not included in the landscape reconstruction onshore Scandinavia. The  
243 result is a landscape representing a pre-glacial state before any major glaciations in Scandinavia, featuring a  
244 large submarine depression in the North Sea and a much narrower continental shelf along the Norwegian  
245 margin than at present (Fig. 2a,c). In addition to the PREQ experiment two sub-experiments are presented:  
246 ‘PREQ-onshore’ where only the onshore fjord erosion has been reconstructed (material added compared to  
247 present-day) and ‘PREQ-offshore’ where only the offshore deposition has been reconstructed (material  
248 removed compared to present-day). Neither of these additional sub-experiments considers the offshore  
249 sediment wedge on the shelf. With the sub-experiments we can assess which processes control the behaviours  
250 and ice volume changes observed in the PREQ experiment.

251

252 For the middle/late Quaternary (MLQ) experiment, we reconstruct the bathymetry by estimating the volumes  
253 of erosion that have been carved into the modern-day sea-bed by ice streams on the Norwegian shelf and in  
254 the Norwegian Channel (Fig. 1). This bathymetric erosion is estimated using the geophysical relief method  
255 (e.g., Steer et al., 2012; Pedersen et al., 2021) on the present-day GEBCO 2022 global DEM (GEBCO  
256 Bathymetric Compilation Group., 2022), using a grid resolution of 1 x 1 km and a sliding window radius of  
257 35 km. The resulting filled bathymetry, that also fills fjords to sea level, is adjusted with the flexural isostatic  
258 response to loading using gFlex 1.1.1 (Wickert, 2016) with an effective elastic thickness of 15 km. This  
259 reconstruction of the Scandinavian morphology is meant to represent a state before the formation of the  
260 Norwegian Channel (Fig. 2b,d) and could represent an age of approximately ~0.5 Ma. This approximate age  
261 is supported by the presence of buried mega-scale glacial lineations and drumlins in stratigraphic sequences  
262 of the North Sea suggesting that grounded ice has been present since ~0.5 Ma, whereas the lack of these  
263 features in the older strata indicate that early Quaternary glaciations did not ground, but only supplied icebergs  
264 to the North Sea (Dowdeswell and Ottesen, 2013; Rea et al., 2018).

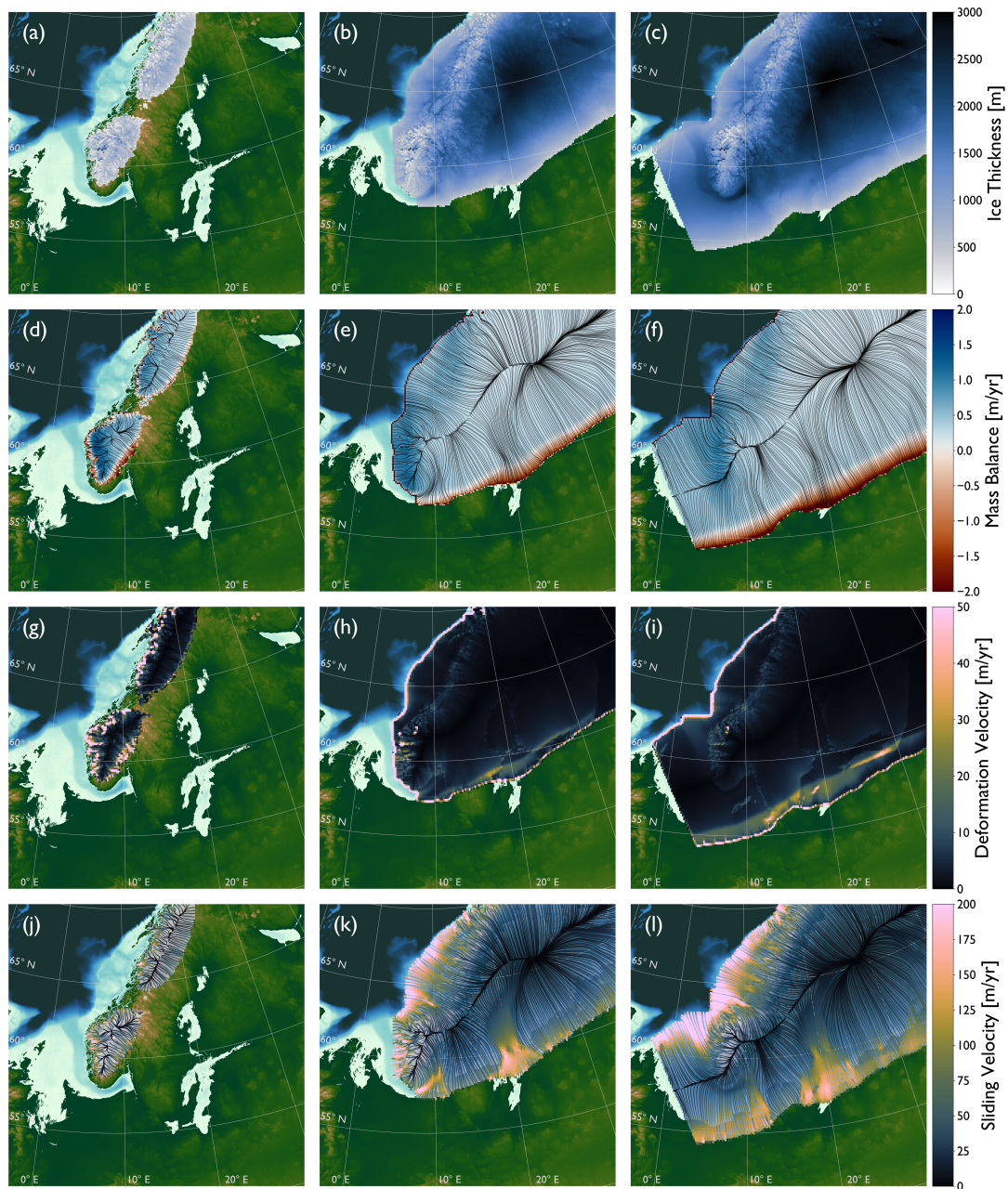
265

266 **3 Results**

267 In this section we start by presenting the results from our reference model simulating the evolution of the SIS  
268 on the present-day topography and bathymetry over the last glacial period. Then we present the results of our  
269 two experiments with reconstructed topography and bathymetry and how they differ from the reference model.  
270 Lastly, we present our findings regarding ~~a possible timing~~the of formation ~~for~~of the Norwegian Channel.  
271  
272  
273  
274  
275  
276  
277  
278  
279  
280  
281  
282  
283  
284  
285  
286  
287  
288  
289

290

291



292

293 **FIG. 3.** Model output from three time slices of the reference experiment, left column: early glaciation (72  
 294 ka), middle column: late-intermediate glaciation (22 ka), right column: glacial maximum (17 ka). a-c) ice  
 295 thickness, d-f) mass balance, g-i) depth averaged deformation velocity and j-l) sliding velocity.

296

297

298

299

300



301

### 302 3.1 Reference model

303 To illustrate the spatial and temporal development of the SIS in our model simulations, we present model  
304 output from three snapshots in time (Fig. 3): minor ice build-up during early glaciation (72 ka), moderate  
305 glacial build-up during intermediate times of the glaciation (22 ka), and glacial maximum that happens in these  
306 simulations at 17 ka. We note that the delayed timing of glacial maximum ~~timing~~ in our models compared to  
307 the timing of the reconstructed maximum extent in Scandinavia (~21-19 ka, Hughes et al., 2016) is a direct  
308 consequence of the chosen climate forcing, utilizing a glaciation index that peaks at 18 ka. We do not intend  
309 here to match the exact timing of the maximum extent (LGM). During our simulated early glaciation, ice extent  
310 is limited to mountain regions with high topography and high latitude regions in Norway and Sweden (Fig.  
311 3a). Mass balance is positive ~1.5 m/yr in high altitude regions at the Norwegian coast where precipitation is  
312 high, and temperatures are low (Fig. 3d). Ice deformation and sliding is high up to >50 m/yr and >200 m/yr  
313 respectively, during early glaciation (Fig. 3g,j), where ice is thin and controlled by the underlying topography  
314 that includes mountainous regions dissected by fjords and valleys.

315

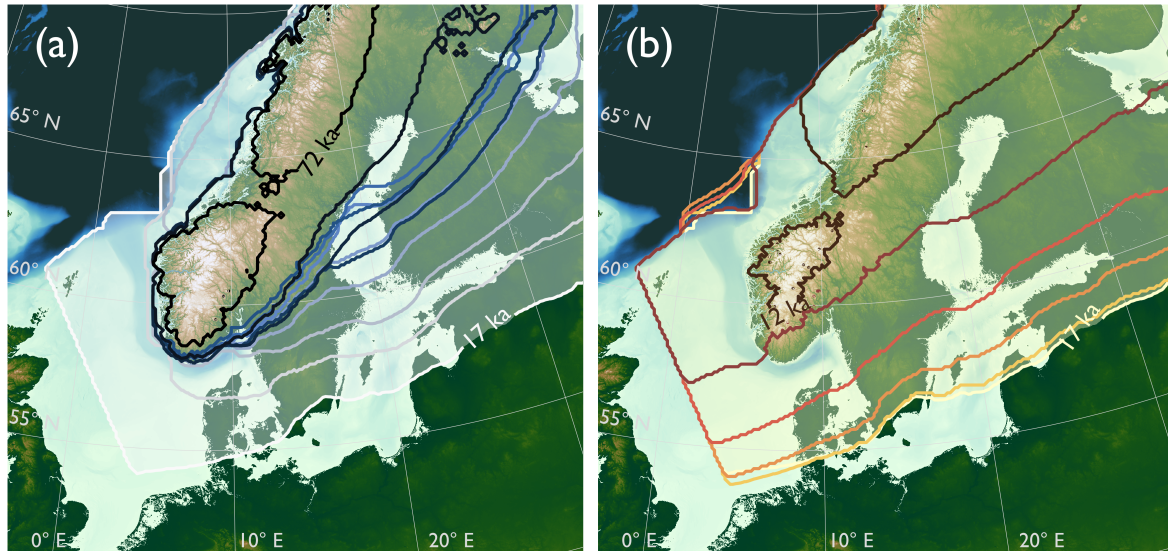
316 During the intermediate glaciation, the ice sheet has advanced onto the shelf region, with grounded ice on the  
317 Norwegian margin, and the ice sheet has started to advance into the North Sea through the inner part of the  
318 Norwegian Channel (Fig. 3b). The mass balance reaches ~1 m/yr at the west coast of Norway (Fig. 3e), with  
319 values across most of the ice sheet <0.5 m/yr, and negative mass balance at the south/western margin reaching  
320 ~-2 m/yr where the ice is thin and velocities exceed ~200 m/yr (Fig. 3h,k). Along the coastal margin to the  
321 west, the mass balance is negative in a narrow zone where floating ice is melting fast. Sliding is notably high,  
322 reaching >200 m/yr in the inner parts of the Norwegian Channel (Fig. 3k). The ice flow is still steered by  
323 topography in the high regions of Southern Norway; ~~and also~~ and in the Bothnic Bay, whereas the main divide  
324 in Northern Scandinavia has shifted east, being largely independent of the underlying topography (Fig. 3e).

325

326 During glacial maximum, the ice sheet reaches a thickness of >3000 m in the central parts (Fig. 3c) with a  
327 relatively low positive mass balance along the west coast of Norway (<1 m/yr; Fig. 3f) with the same general  
328 spatial pattern in accumulation and ablation as the intermediate glaciation (Fig. 3e) across the ice sheet ~~as~~  
329 ~~during the intermediate glaciation~~. Sliding is high along the northeastern-northwestern margin of the ice sheet  
330 (>200 m/yr) especially near the shelf break where ice is funnelled towards the deeper ocean (Fig. 3l). For a  
331 while (~5,000 yrs) during the maximum expansion, the ice sheet merges with the BIIS in the western part of  
332 the North Sea, simulated as an ice wall (Fig. 3f,l). At this time, the ice flow rearranges into a divergent pattern  
333 from the ice saddle that emerges between the BIIS and the SIS. Consequently, the ice flows across the  
334 Norwegian Channel during the maximum extent ~~of the ice sheet~~ instead of being focused in the channel itself,  
335 as the ice is diverged southward, driven by the surface slope of the ice sheet under this ice configuration (Fig.  
336 3l). It is worth noting that the reference model captures a realistic placement of the LGM ice divide (Fig. 3f)  
337 in accordance with geological observations (Fig. 1; Olsen et al., 2013). Additionally, the ice divide of the  
338 saddle across the North Sea during glacial maximum, when the SIS merges with the BIIS, closely resembles



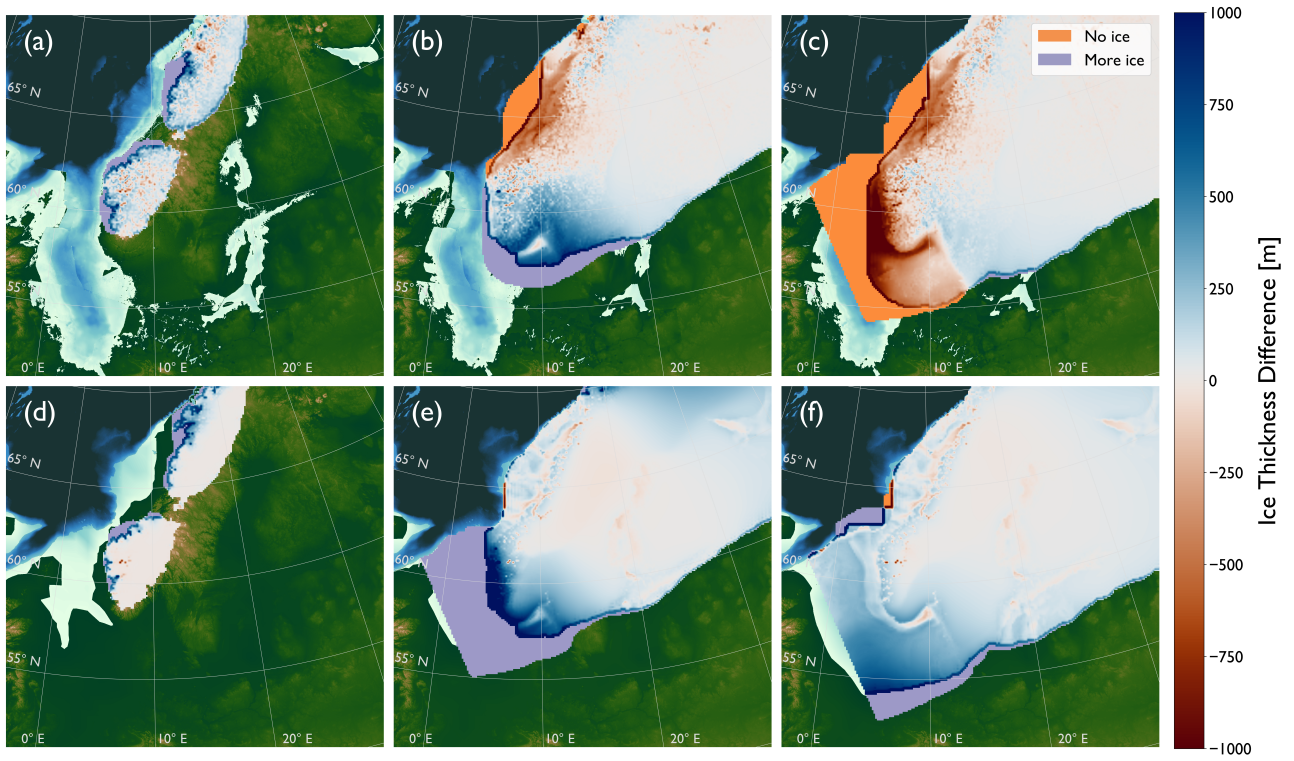
339 [the ice divide suggested by Clark et al. \(2022\) using a combination of observations and modelling techniques.](#)  
340 The glacial maximum ice extent in our reference experiment is within the maximum LGM ice extent (Fig. 1;  
341 Hughes et al., 2016), albeit with less ice towards the southern margin and more ice in northeast.  
342  
343



344  
345 **FIG. 4. Advance and retreat of the SIS in the reference experiment. A) ice advance in 5 kyr intervals between**  
346 **model years 72 ka and 17 ka. B) retreat in 1 kyr intervals from 17 to 12 ka.**  
347

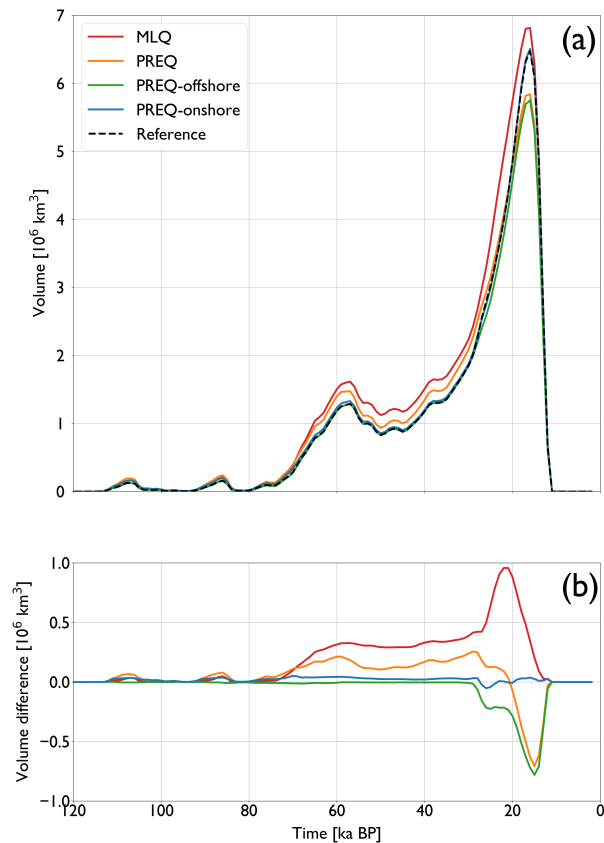
348 Buildup of the SIS from early mountain glaciation to glacial maximum happens gradually with grounded ice  
349 on the Norwegian shelf forming 10,000 model years before glacial maximum, and ice advance in the North  
350 Sea occur over just 5000 model years approaching glacial maximum extent (Fig. 4A). In contrast, the ice  
351 retreat is rapid with ice mass loss from the glacial maximum back to a state similar ~~to~~as early glaciation  
352 happening over just 5000 model years (Fig. 4B).  
353  
354  
355  
356  
357  
358  
359  
360  
361  
362  
363  
364

365  
366  
367  
368  
369  
370



371 **FIG. 5.** Differences in ice thickness for the a,b,c) PREQ and d,e,f) MLQ experiments compared to the  
372 reference experiment *for the same time slices as Fig. 3*. Blue colors means more ice in this experiment than  
373 the reference experiment and red colors means less ice.

374  
375  
376  
377  
378  
379  
380  
381  
382  
383  
384  
385  
386



387

388

389

390

391

392

393

394

395

396

397

398

399

**FIG. 6. a) ice volume over time for the different experiments, b) volume differences between the different experiments and the reference experiment. The black dashed line in a) is the reference model, the red line is the mid/late Quaternary experiment, and the yellow line is the early Quaternary experiment. The green and blue lines represent the two sub-experiments of the early Quaternary experiment (offshore and onshore landscape changes compared to present day, respectively).**

400

### 3.2 Results from PREQ and MLQ

401

In the model simulation representing ice-sheet behavior on an early Quaternary landscape morphology (PREQ; Fig. 2a, Fig. 5a-c), the ice sheet initially extends further than the reference model (Fig. 5a, purple color), particularly towards the Norwegian coast. At the intermediate stage (Fig. 5b), the ice sheet shows a smaller extent and thickness towards the Norwegian margin (Fig. 5b, orange color), whereas the ice extends further towards the south (Fig. 5b, purple color) with an ice thickness increase of  $>500$  m in some regions. The location of the present-day Norwegian Channel shows a much thinner ice since this bathymetric depression is not present in the PREQ landscape reconstruction (Fig. 5b). At the maximum extent, the ice sheet is smaller both

407

408 along the western and the southwestern margins (Fig. 5c, orange color), with a general decrease in ice sheet  
409 thickness compared to the reference model (Fig. 5c, red colors). The reduced extent and ice ~~volume~~-thickness  
410 during the maximum extent result in ~10 % lower maximum ice volume than the reference model (Fig. 6,  
411 orange curve). The large difference in ice volume between the PREQ experiment and the reference experiment  
412 is largely driven by differences in bathymetry (PREQ-offshore; Fig. 6a, green curve) as changes in topography  
413 do not lead to significant differences in ice volume compared to the reference model (PREQ-onshore, Fig. 6a,  
414 blue ~~line~~curve)

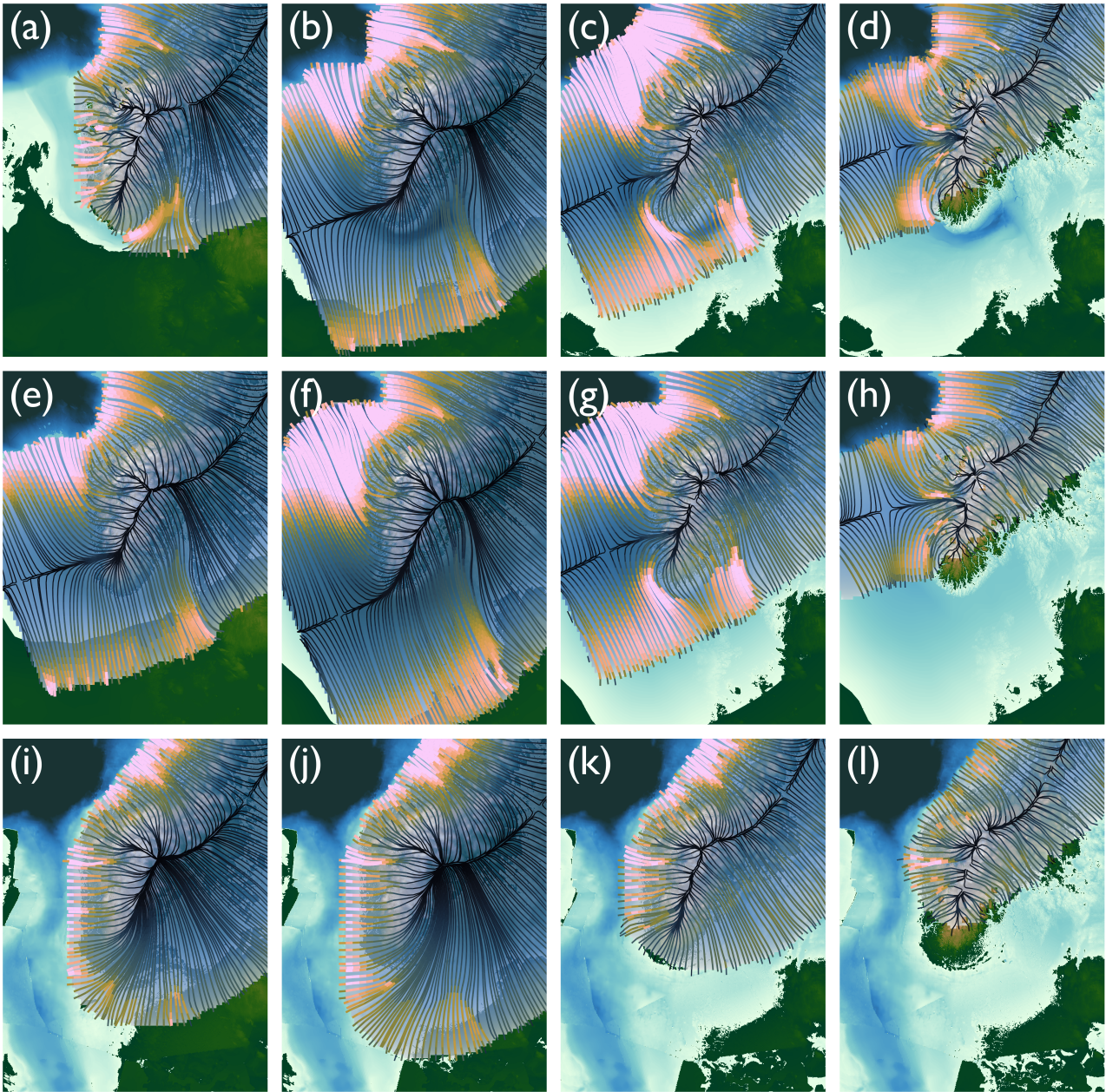
415  
416  
417 For the MLQ simulation that represents ice flow on a landscape morphology that existed prior to extensive  
418 erosion of the bathymetry by ice streaming (Fig. 2b, Fig. 5d-f), the ice sheet also starts slightly larger (Fig. 5d,  
419 purple color) compared to the reference model. At the intermediate stage, the ice sheet has already extended  
420 all the way across the North Sea (Fig. 5e, purple color), showing also a significantly thicker ice sheet in the  
421 adjoining regions onshore Scandinavia. This trend is continued during the maximum extent, where the MLQ  
422 ice sheet extends even further, particularly towards the south (Fig. 5f, purple colors). In general, the extent of  
423 the MLQ ice sheet is not changed along the Norwegian margin, where the width of the shelf has not changed  
424 for this simulation (Fig. 5e-f). The increased ice extent and ice thickness in the MLQ simulation result in a  
425 maximum ice volume that is ~25 % more than the reference model during intermediate stage and ~5 % during  
426 the glacial maximum as a direct result of the changed bathymetry (Fig. 6, red ~~line~~curve).

### 428 3.3 Sliding in the Norwegian Channel

429 The erosive power of ice is a product of ice flux over a region with grounded ice (Patton et al. 2022) and is  
430 strongly correlated with ice sliding velocity (Cook et al. 2020), which means sliding velocity can be considered  
431 a proxy for erosive potential. Here we explore whether our higher-order ice-sheet model can capture the erosive  
432 potential through sliding in the Norwegian Channel in the present-day bathymetry of the reference model and  
433 whether the model can predict erosion when the channel is not there in the PREQ and MLQ experiments. The  
434 ice dynamics in our reference simulation show significant sliding in the Norwegian Channel in four distinct  
435 phases (Fig. 7a-d). In the early glacial stage, the ice is sliding fast southeast of southern Norway along the  
436 deepest part of the channel (Fig. 7a). As the ice approaches maximum extent, the sliding pattern changes  
437 because of the different ice flow patterns that arise as an ice saddle emerges in the North Sea when the SIS  
438 merges with the BIIS (Fig. 7b). At this stage, ice flows south across the channel from the southern mountains  
439 of Norway, following the steepest surface gradient of the ice sheet. Instead, sliding is now mostly concentrated  
440 in the outer parts of the Norwegian Channel close to the North Sea Fan (Fig. 7b).-During retreat, ice sliding  
441 continues in the outer parts of the channel, but also becomes prominent along the southern tip of Norway with  
442 ice sliding towards the southeast, and in the inner parts of the channel near Oslo Fjord (Fig. 7c). Finally, as the  
443 ice sheet retreats further, continued sliding toward the North Sea Fan is complemented by a phase of southward  
444 sliding in the channel along the south-western coast, a region that had not seen significant prior sliding (Fig.  
445 7d). In ~~F~~figure 7e-h we show the same time slices for the MLQ experiment. Here, the ice extends further

446 towards the west and has already formed a saddle between the SIS and the BIIS during the initial phase of the  
447 glacial cycle (Fig. 7e), and sliding is high towards the shelf break in the region that will later become the  
448 outermost part of the Norwegian Channel. Sliding velocities towards the shelf break are consistently high  
449 throughout the model simulation (Fig. 7f,h), whereas sliding accelerates in the inner parts of what will become  
450 the Norwegian Channel during ice retreat (Fig. 7g). In the last time slice, sliding velocity is lower than the  
451 reference experiment but has the same general pattern (Fig. 7h), with sliding in some regions along the west  
452 coast of Southern Norway. In figure 7i-l we present the time slices for the PREQ experiment. Across all four  
453 panels the patterns differ from the reference and MLQ experiments. Instead, we observe high sliding velocities  
454 towards the west across where the channel is today (Fig. 7i-k). In the last time slice we observe very little  
455 sliding as the ice has retreated mostly onshore at this time in the PREQ experiment (Fig. 7l).  
456  
457  
458





459

460

461 **FIG. 7. Sliding velocity in southwestern Norway for reference model year a) 23 ka, b) 17 ka, c) 14 ka, and**  
 462 **(d) 13 ka. *Same color scale as Fig. 3j-l.* Same for MLQ experiment e-h and PREQ experiment i-l.**

463

464

465

#### 466 4. Discussion

##### 467 4.1 Ice extent and volume

468 ~~The volume of ice contained in the Scandinavian ice sheet at LGM is estimated to be between  $5.3-6.5 \cdot 10^6 \text{ km}^3$~~   
 469 ~~(Hughes et al. 2016). This is in good agreement with our~~ The ice volume in our reference experiment ~~that~~  
 470 reaches  $6.5 \text{ M km}^3$  at glacial maximum, which is within estimates of SIS and Eurasian ice sheet volume from

471 [previous studies \(e.g., Hughes et al., 2016; Patton et al. 2016; Simms et al. 2019\)](#). The ice divide of the SIS in  
472 the reference experiment is in good agreement with observations (Fig. 1, Fig. 3f) which also affirms that our  
473 model captures an adequate representation of the ice sheet during the last glacial period. The differences in  
474 maximum ice extent between our reference experiment and observations (Hughes et al., 2016; Fig. 1) can be  
475 attributed to the simple mass balance implemented in our model using linear gradients that does not capture  
476 the complex nature of the regional climate during the last glacial cycle but is an adequate approximation for  
477 our purposes. Geological observations suggest that the main ice advance in Denmark approaching glacial  
478 maximum between 20-22 ka came from the northeast bringing till deposits of Middle Swedish provenance  
479 (Houmark-Nielsen, 2004), whereas the main ice advance into Denmark in our reference experiment comes  
480 from the north (Fig. 4a). A possible reason that our model does not capture this dynamic in the southerly ice  
481 advance could be the lack of subglacial hydrology in the model which can increase sliding rates (Egholm et  
482 al. 2012a). It could also be the lack of a more complex stress dependent ice viscosity, where the Glen's flow  
483 law stress exponent can increase to  $n \approx 4$  in some areas, which can increase the flow velocity by an order of  
484 magnitude (Millstein et al., 2022). These effects could be important especially in the southern parts of the ice  
485 sheet where the ice is thin and fast flowing during advance (Fig. 3c,i). Here, an even faster and thinner ice  
486 might be more sensitive to the low relief topography of southern Scandinavia leading to a more westerly ice  
487 flow from Sweden into Denmark in agreement with the observations.

488  
489 We cannot directly compare the ice extents in our experiments with reconstructions of past SIS extent as we  
490 use the same climate forcing between experiments, but we can assess whether differences in past ice sheet  
491 extents follow the same trends as we see in this study that is based solely on differences in morphology.  
492 Batchelor et al. (2019) use empirical data to evaluate past northern hemisphere glacial extents, and suggest  
493 best-estimate maximum southern extents of the MIS 12 (429-477 ka), MIS 16 (622-677 ka), and MIS 20-24  
494 (790-928 ka) ice sheets to be somewhere between the best-estimate maximum MIS 6 extent and the LGM  
495 extent (Fig. 1; dashed red line, black line, 132-190 ka), although the MIS 16 and MIS 20-24 maximum ice  
496 sheet extents are highly uncertain. These reconstructions are based on very limited observations and in some  
497 cases (e.g., MIS 12 and 16) the estimates are mostly based on similarities in the  $\delta^{18}\text{O}$  curve (Batchelor et al.,  
498 2019). We show with this study that purely morphological differences in bathymetry between the last glacial  
499 period and  $\sim 0.5$  Ma-~~ka~~ (MLQ experiment, similar in time to MIS 12/16) allow for larger ice-sheet extents  
500 simply owing to geomorphic changes during this time period. This suggests that both climatic and topographic  
501 forcing might have caused these (possibly) large ice extents of the mid-late Quaternary (MIS 12,16,20-24).  
502 Indeed, our results showcase that a smooth bathymetry in the North Sea region (i.e., lacking glacial  
503 morphology), such as before the inception of the Norwegian Channel, could lead to earlier and more extensive  
504 southerly ice advance within a glacial period (Fig. 5e). On the other hand, our simulation of early Quaternary  
505 glaciations suggests that ice buildup across the North Sea was not plausible at this early stage of glacial  
506 landscape evolution. Indeed, in the PREQ experiment we find that the SIS could extend no further than the  
507 continental shelf during the early Quaternary (Fig. 5b,c). This is consistent with a study of buried glacial  
508 landforms in the central North Sea documenting ice-berg plough marks in early Quaternary sediments



509 (Dowdeswell et al., 2013; Rea et al., 2018). Our reconstructed early Quaternary ice sheet would have supplied  
510 icebergs that created these plough marks.

511

512 The differences we find in ice volume at the maximum glacial extent (~5 % higher for MLQ, ~10 % lower for  
513 PREQ), illustrate how differences in morphology affects ice volume independent of the climate forcing. This  
514 has implications for the proxies we use for ice volume history. ~~Looking at the peak values in the LR04 Benthic  
515 Stack for LGM (5.02 ± 0.03 ‰), MIS 6 (4.98 ± 0.05 ‰), MIS 12 (5.08 ± 0.05 ‰), MIS 16 (5.08 ± 0.06 ‰),  
516 and MIS 20-24 (4.69 ± 0.08 ‰), the proportional differences between these  $\delta^{18}\text{O}$  peaks (~1-7 %) are less than  
517 the proportional differences of 5-10% in peak ice volume between the model simulations presented here,  
518 suggesting that landscape evolution can play an important role in controlling ice volume.~~ Clearly the effect of  
519 glacial morphology explored here is local in nature whereas the LR04 Benthic Stack we use as a glacial index  
520 and a proxy for ice volume is a global proxy. In addition, local ice volume also depend on global atmospheric  
521 circulation patterns which can lead to asynchronous development of the ice sheets during a glacial period (e.g.,  
522 Liakka et al., 2016) that will also influence ice-sheet volume between glacial cycles. But landscape evolution  
523 have also played a significant role along other ice-sheet margins through the Quaternary for example leading  
524 to increased ice sheet advance across marine sectors of the Antarctic ice sheet (Hochmuth et al. 2019,2020).  
525 and in addition, local ice volume also depend on global atmospheric circulation patterns which can lead to  
526 asynehronous development of the ice sheets during a glacial period (e.g., Liakka et al., 2016) that will also  
527 influence ice-sheet volume between glacial cycles. It should also be noted that the lack of ice shelves in our  
528 model could have a significant impact on grounded ice volume as buttressing effects of ice shelves can stabilize  
529 and advance grounding lines across the marine sectors of an ice sheet (e.g., Gasson et al. 2018). ~~Nevertheless,  
530 a~~ Nevertheless, according to this study landscape morphology alone can account for up to ~10 % (~25% during  
531 ice build-up) difference in ice volume between glacial cycles for the Scandinavian region (~25 % during ice  
532 build-up), implying that glacial landscape evolution could be an overlooked mechanism impacting local and  
533 global ice volume and thereby the interpretation of  $\delta^{18}\text{O}$  values curves. This emphasizes the added uncertainty  
534 of landscape morphology on Quaternary ice sheet reconstructions.

535

## 536 4.2 Formation of the Norwegian Channel

537 It is uncertain how and when the Norwegian Channel was formed, with studies estimating the time of formation  
538 to be between ~0.35-1.1 Ma – with more recent studies suggesting younger ages (e.g., Sejrup et al., 2003;  
539 Hjelstuen et al., 2012; Løseth et al., 2022). In this study, we have assumed that the entirety of the Norwegian  
540 Channel formed after ~0.5 Ma (MLQ).

541

542 For the last glacial cycle, it has previously been proposed that the Norwegian Channel Ice Stream (NCIS) was  
543 active in stages but mainly during the LGM (e.g., Sejrup et al., 1998; Sejrup et al., 2003). According to an  
544 earlier study (Sejrup et al., 2016), ice streaming in the outer parts of the channel near the shelf break started  
545 close to the LGM with increased activity promoting ice retreat around 19 ka because of increased ice mass  
546 loss. The retreat translated southwards over time as the SIS unzipped from the adjacent BIIS after which ice

547 streaming was mostly confined to the main trunk of the channel (Sejrup et al., 2016). A previous modelling  
548 study also suggests that the NCIS was active in stages with streaming in the inner parts of the channel leading  
549 up to, and deactivated during, glacial maximum because of the saddle forming from the merging of the BIIS  
550 and the SIS (Boulton and Hagdorn, 2006). ~~In that study, the NCIS was mostly active near the shelf break at~~  
551 ~~LGM and during retreat the ice stream funnelled ice along the entire length of the Norwegian Channel (Boulton~~  
552 ~~and Hagdorn, 2006).~~ We find in this study our reference model with present day bathymetry, that ice streaming  
553 was active in the inner parts of the channel before the saddle formed between the BIIS and the SIS, after which  
554 ice streaming velocity increased dramatically in the outer parts of the Norwegian Channel near the shelf break  
555 and ~~mostly~~ deactivated in the inner parts of ~~T~~the Norwegian Channel as the saddle formed, consistent with  
556 other literature based on observations of e.g. subglacial landforms combined with dated sediment cores (Sejrup  
557 et al., 2016). ~~However~~ On the other hand, our reference experiment does not mimic at any time an NCIS  
558 spanning the entire trunk of the Norwegian Channel, which would significantly contribute to ice mass loss  
559 from rapid grounding line retreat as is supported by observations (Sejrup et al., 2016). ~~However, w~~We cannot  
560 with this model setup rule out the occurrence of continuous ice streaming in the entire Norwegian Channel  
561 after the LGM. Indeed, some processes central to reproducing realistic ice stream behaviour ~~is~~ are not included  
562 in iSOSIA, ~~including such as~~ enhanced basal melt owing to basal friction, leading to accelerated thinning in  
563 regions with rapid ice sliding as well as effects of internal friction and temperature advection on ice viscosity  
564 which can greatly amplify sliding velocities (Millstein et al., 2022; Bondzio et al., 2016). These mechanisms  
565 could contribute to highly elevated sliding velocities, especially in the NCIS, and could facilitate a propagation  
566 of the streaming activity we observe in the outer parts of the channel to the inner parts. In addition, the static  
567 ice wall we use to simulate the merging SIS and BIIS introduces a highly persistent ice saddle, that may  
568 introduce unrealistic streaming patterns and ice extent during NCIS retreat (Fig. 7c,d,g,h). Indeed, a previous  
569 study facilitates the retreat of the Norwegian Channel with a negative SMB anomaly in the southern sector of  
570 the North Sea, in order to match the ice margin to empirical reconstructions (Gandy et al. 2021).

571  
572 ~~Despite the channel being filled with sediment in the reconstructed bathymetry in the MLQ experiment we~~  
573 ~~find an ice streaming pattern similar to that of the reference model, with even higher sliding in the outer parts~~  
574 ~~of the Norwegian Channel from 23–17 ka near the shelf break because of the faster advance in the North Sea~~  
575 ~~in this experiment. In the PREQ experiment streaming is limited to a pattern across channel towards the west~~  
576 ~~because of the sediment wedge sloping along the shoreline leading the ice towards the middle North Sea. We~~  
577 ~~find it likely that the channel could initially have been formed during multiple glacial periods since ~0.5 Ma~~  
578 ~~before the main formation occurred in recent glacial periods (~0.35 Ma; Løseth et al. 2022). This would be in~~  
579 ~~agreement with studies on the North Sea Fan (NCIS depocenter), suggesting that 90% of the sediments in this~~  
580 ~~fan are younger than 0.5 Ma (Hjelstuen et al., 2012).~~——

581  
582 Despite the Norwegian Channel being filled with sediment in the reconstructed bathymetry of our MLQ  
583 experiment, we find an ice streaming pattern that are comparable to that of the reference model for several  
584 parts of the model (Fig. 7, a-h). Specifically, in the MLQ experiment, high sliding velocities are also present

585 in what will become the inner part of the Norwegian Channel as the ice begins to advance offshore  
586 (Supplementary video 3), although less focused compared to the reference model where the depression of the  
587 Norwegian Channel steers the ice even further (Fig. 7a). We stress however, that because the ice advances  
588 faster offshore in the MLQ experiment, this sliding in the inner parts of what will become the Norwegian  
589 Channel happens prior to 23 ka (Fig. 7e, Supplementary Video 3). The MLQ experiment also shows high  
590 sliding rates where the outer part of the Norwegian Channel will form towards the shelf break (Fig. 7e-h), even  
591 extending further back in time than the reference experiment (Fig. 7a,e). This steering of ice towards the NNW  
592 in the MLQ experiment that takes place before a bathymetric depression is formed, is mainly controlled by the  
593 steeper ice-surface gradient that arise toward the shelf break in this simulation, when the ice advances into the  
594 offshore and approaches the shelf break much earlier than in the reference experiment. This ice-flow pattern  
595 begins before the saddle between the BIIS and the SIS formed, but is amplified further by the ice saddle that  
596 forms in the North Sea as the ice cannot advance further toward the west (Supplementary Video 3). Our models  
597 can thus explain the initial formation of the Norwegian Channel in the innermost and outermost parts, starting  
598 from a bathymetry that had no prior imprint of the present-day channel. The MLQ experiment also show  
599 sliding in other parts of what will become the Norwegian Channel later in the model simulation (e.g., Fig. 7g-  
600 h). However, we find these results less robust owing to the limitations of our model setup during the  
601 deglaciation.

602  
603 On the other hand, the PREQ experiment show no ice flow and sliding patterns similar to the reference model,  
604 in the region that would later become the Norwegian Channel. Indeed, ice flow and sliding is at all times  
605 perpendicular to the future Norwegian Channel because of the sediment wedge that existed along the  
606 Norwegian coast and a steep ice-surface gradient towards the North Sea, sustained by the deep bathymetry of  
607 the North Sea that prevented grounded ice. Therefore, we find it likely that the carving of the Norwegian  
608 Channel could not have been initiated before the North Sea basin had been sufficiently filled with sediments.  
609 Instead, we find it plausible that the Norwegian Channel formed during multiple glacial periods since ~0.5 Ma  
610 consistent with a recent study indicating that the channel was formed prior to ~0.35 Ma (Løseth et al. 2022).  
611 Our results are also in agreement with studies on the North Sea Fan (NCIS depocenter), suggesting that 90%  
612 of the sediments in this fan are younger than ~0.5 Ma (Hjelstuen et al., 2012).

613

## 614 **5. Conclusion**

615 We have used a higher-order ice sheet model to investigate the effect of landscape morphology on the SIS  
616 evolution and dynamics. Three different experiments were conducted: (i) a reference experiment resembling  
617 the last glacial cycle using modern-day topography and bathymetry, (ii) a mid-late-Quaternary (MLQ)  
618 experiment with glacial morphological features in the present-day bathymetry filled with sediment, and (iii) a  
619 pre-Quaternary (PREQ) experiment, simulating the SIS on a reconstructed pre-glacial topography and  
620 bathymetry. We find in the MLQ experiment that removing glacial morphological features in the bathymetry  
621 allows for faster and further southward expansion at similar climatic conditions allowing for a larger ice sheet.  
622 On the contrary we find in the PREQ experiment that the early Quaternary bathymetry did not allow for the



623 SIS to advance as far westward and southward, thereby limiting the size of early glaciations and preventing a  
624 merge of between the BIIS and the SIS. Looking at the prominent glacio-morphological feature, the  
625 Norwegian Channel, we find that the PREQ experiment does not allow for significant ice streaming in this  
626 area and that the channel was more likely formed since ~0.5 Ma after the North Sea was filled in with glacial  
627 sediments. Furthermore, our results suggest ice streaming occurred in distinct stages along the trunk of the  
628 channel with high ice sliding in the inner parts before LGM and sliding in the outer parts of the channel close  
629 to the shelf break during LGM. Our results also show that sliding in the inner parts of the channel deactivated  
630 because of divergent ice flow when the BIIS and the SIS merged and formed a saddle across the North Sea.

631

## 632 **6. Code/Data availability**

633 Code and/or data will be made available upon request.

## 634 **7. Author contribution**

635 Gustav Jungdal-Olesen: Conceptualization, Methodology, Software, Formal analysis, Writing, original draft,  
636 Visualization. Vivi K. Pedersen: Conceptualization, Methodology, Supervision, Writing, review & editing,  
637 Funding acquisition. Jane L. Andersen: Writing, review & editing, Visualization. Andreas Born: Resources,  
638 Writing, review & editing

639

## 640 **8. Competing interests**

641 The authors declare that they have no conflict of interest.

642

## 643 **9. References**

644

645 Anderson, R. S., Dühnforth, M., Colgan, W. & Anderson, L. Far-flung moraines: Exploring the feedback of  
646 glacial erosion on the evolution of glacier length. *Geomorphology* 179, 269–285 (2012).

647

648 Bart, P.J., Mullally, D., Gollledge, N.R., 2016. The influence of continental shelf bathymetry on

649 antareticAntarctic ice sheet response to climate forcing. *Global and Planetary Change* 142, 87–95. URL:

650 <http://dx.doi.org/10.1016/j.gloplacha.2016.04.009>, doi:10.1016/j.gloplacha.2016.04.009.

651

652 Batchelor, C.L., Margold, M., Krapp, M., Murton, D.K., Dalton, A.S., Gibbard, P.L., Stokes, C.R., Murton,  
653 J.B., Manica, A., 2019. The configuration of northern hemisphere ice sheets through the Quaternary. *Nature*  
654 *Communications* 10, 3713. URL: <http://www.nature.com/articles/s41467-019-11601-2>, doi:10.1038/s41467-  
655 019-11601-2.

656

657 Binzer, K., Stockmarr, J., Lykke-Andersen, H., 1994. Pre-quaternary Surface Topog- raphy of  
658 denmarkDenmark. Geological survey of denmarkDenmark map series no. 44.

659

660 Bondzio, J.H., Morlighem, M., Seroussi, H., Kleiner, T., Rückamp, M., Mougintot, J., Moon, T., Larour, E.Y.,  
661 Humbert, A., 2017. The mechanisms behind jakobshavn isbræ's acceleration and mass loss: A 3-d  
662 thermomechanical model study. *Geophysical Research Letters* 44, 6252–6260. Doi:10.1002/2017GL073309.  
663

664 Boulton, G., Hagdorn, M., 2006. Glaciology of the british isles ice sheet during the last glacial cycle: form,  
665 flow, streams and lobes. *Quaternary Science Reviews* 25, 3359–3390. Doi:10.1016/j.quascirev.2006.10.013.  
666

667 Clague, J.J., Barendregt, R.W., Menounos, B., Roberts, N.J., Rabassa, J., Martinez, O., Ercolano, B., Corbella,  
668 H., Hemming, S.R., 2020. Pliocene and early ~~pleistocene~~Pleistocene glaciation and landscape evolution on the  
669 ~~patagonian~~Patagonian steppe, santa cruz province, ~~argentina~~Argentina. *Quaternary Science Reviews* 227,  
670 105992. Doi: ~~https://doi.org/~~10.1016/j.quascirev.2019.105992.  
671

672 Clark, C. D., Ely, J. C., Hindmarsh, R. C. A., Bradley, S., Ignéczi, A., Fabel, D., Ó Cofaigh, C., Chiverrell, R.  
673 C., Scourse, J., Benetti, S., Bradwell, T., Evans, D. J. A., Roberts, D. H., Burke, M., Callard, S. L., Medialdea,  
674 A., Saher, M., Small, D., Smedley, R. K., ... Wilson, P. (2022). Growth and retreat of the last British–Irish Ice  
675 Sheet, 31 000 to 15 000 years ago: the BRITICE-CHRONO reconstruction. *Boreas*, 51(4), 699–758.  
676 <https://doi.org/10.1111/bor.12594>  
677

678 Cook, S.J., Swift, D.A., Kirkbride, M.P., Knight, P.G., Waller, R.I., 2020. The empirical basis for modelling  
679 glacial erosion rates. *Nature Communications* 11. Doi:10.1038/s41467-020-14583-8.  
680

681 Dee, D., National Center for Atmospheric Research Staff (Eds). Last modified 2022-11-07 †The Climate Data  
682 Guide: ERA-Interim.† Retrieved from <https://climatedataguide.ucar.edu/climate-data/era-interim>  
683 on 2023-08-27.  
684

685 Dowdeswell, J.A., Ottesen, D., 2013. Buried iceberg ploughmarks in the early quaternary sediments of the  
686 central north sea: A two-million year record of glacial influence from 3d seismic data. *Marine Geology* 344,  
687 ~~1-9~~1-9. URL: <http://dx.doi.org/10.1016/j.margeo.2013.06.019>, doi:10.1016/j.margeo.2013.06.019.  
688

689 Egholm, D.L., Jansen, J.D., BrÊdstrup, C.F., Pedersen, V.K., Andersen, J.L., Ugelvig, S.V., Larsen, N.K.,  
690 Knudsen, M.F., 2017. Formation of plateau landscapes on glaciated continental margins. *Nature Geoscience*  
691 10, ~~592-597~~592-597. Doi:10.1038/NGEO2980.  
692

693 Egholm, D.L., Knudsen, M.F., Clark, C.D., Lesemann, J.E., 2011. Modeling the flow of glaciers in steep  
694 terrains: The integrated second-order shallow ice approximation (isosia). *Journal of Geophysical Research:*  
695 *Earth Surface* 116, ~~161-16~~161-16. Doi:10.1029/2010JF001900.  
696

697 Egholm, D.L., Nielsen, S.B., Pedersen, V.K., Lesemann, J.E., 2009. Glacial effects limiting mountain height.

698 Nature 460, ~~884~~887884-887. Doi:10.1038/nature08263.

699

700 Egholm, D.L., Pedersen, V.K., Knudsen, M.F., Larsen, N.K., 2012a. Coupling the flow of ice, wa-  
701 ter, and sediment in a glacial landscape evolution model. *Geomorphology* 141-142, ~~47~~6647-66. ~~URL:~~  
702 ~~<http://dx.doi.org/10.1016/j.geomorph.2011.12.019>~~, doi:10.1016/j.geomorph.2011.12.019.

703

704 Egholm, D.L., Pedersen, V.K., Knudsen, M.F., Larsen, N.K., 2012b. On the importance of  
705 higher order ice dynamics for glacial landscape evolution. *Geomorphology* 141-142, ~~67~~8067-80. ~~URL:~~  
706 ~~<http://dx.doi.org/10.1016/j.geomorph.2011.12.020>~~, doi:10.1016/j.geomorph.2011.12.020.

707

708 Ewing, M., Donn, W.L., 1956. A theory of ice ages. *Science* 123, 1061–1066.  
709 Doi:10.1126/science.123.3207.1061.

710

711 Gandy, N., Gregoire, L. J., Ely, J. C., Cornford, S. L., Clark, C. D., & Hodgson, D. M. (2021). Collapse of the  
712 Last Eurasian Ice Sheet in the North Sea Modulated by Combined Processes of Ice Flow, Surface Melt, and  
713 Marine Ice Sheet Instabilities. *Journal of Geophysical Research: Earth Surface*, 126(4).  
714 <https://doi.org/10.1029/2020JF005755>

715

716 Gasson, E. G. W., Deconto, R. M., Pollard, D., & Clark, C. D. (2018). Numerical simulations of a kilometre-  
717 thick Arctic ice shelf consistent with ice grounding observations. *Nature Communications*, 9(1).  
718 <https://doi.org/10.1038/s41467-018-03707-w>

719

720 GEBCO Bathymetric Compilation Group 2022., 2022. The GEBCO\_2022 Grid — a continuous terrain model  
721 of the global oceans and land. NERC EDS British Oceanographic Data Centre NOC. Doi:10.5285/e0f0bb80-  
722 ab44-2739-e053-6c86abc0289c

723

724 Gladstone, R., Moore, J., Wolovick, M., and Zwinger, T.: Sliding conditions beneath the Antarctic Ice Sheet,  
725 EGU General Assembly 2020, Online, ~~4~~84-8 May 2020, EGU2020-7038, <https://doi.org/10.5194/egusphere-egu2020-7038>, 2020

726

727

728 Goledowski, B., Nielsen, S.B., Clausen, O.R., 2012. Patterns of ~~eneozoie~~Cenozoic sediment flux from western  
729 ~~seandinavia~~Scandinavia. *Basin Research* 24, ~~377~~400377-400. Doi:10.1111/j.1365-2117.2011.00530.x.

730

731 Hall, A.M., Ebert, K., Kleman, J., Nesje, A., Ottesen, D., 2013. Selective glacial erosion on the  
732 ~~norwegian~~Norwegian passive margin. *Geology* 41, ~~1203~~12061203-1206. Doi:10.1130/G34806.1.

733

734 Han, H.K., Gomez, N., Pollard, D., DeConto, R., 2021. Modeling northern hemispheric ice sheet dynamics,  
735 sea level change, and solid earth deformation through the last glacial cycle. *Journal of Geophysical Research:*  
736 *Earth Surface* 126, ~~44–51~~1–15. Doi:10.1029/2020JF006040.

737

738 Hjelstuen, B.O., Nygard, A., Sejrup, H.P., Hafliðason, H., 2012. Quaternary denudation of southern fennoscandia  
739 — evidence from the marine realm. *Boreas* 41, ~~379–390~~379–390. Doi:10.1111/j.1502-3885.2011.00239.x.

740

741 Hochmuth, K., & Gohl, K. (2019). Seaward growth of Antarctic continental shelves since establishment of a  
742 continent-wide ice sheet: Patterns and mechanisms. *Palaeogeography, Palaeoclimatology, Palaeoecology*, 520,  
743 44–54. <https://doi.org/10.1016/j.palaeo.2019.01.025>

744

745 Hochmuth, K., Gohl, K., Leitchenkov, G., Sauermilch, I., Whittaker, J. M., Uenzelmann-Neben, G., Davy, B.,  
746 & de Santis, L. (2020). The Evolving Paleobathymetry of the Circum-Antarctic Southern Ocean Since 34 Ma:  
747 A Key to Understanding Past Cryosphere-Ocean Developments. *Geochemistry, Geophysics, Geosystems*,  
748 21(8). <https://doi.org/10.1029/2020GC009122>

749

750 Houmark-Nielsen, M., 2004. The Pleistocene of Denmark: a review of stratigraphy and glaciation history. pp.  
751 ~~35–46~~35–46. URL: <https://linkinghub.elsevier.com/retrieve/pii/S1571086604800551>, doi:10.1016/S1571-  
752 0866(04)80055-1.

753

754 Hughes, A.L., Gyllencreutz, R., ystein S. Lohne, Mangerud, J., Svendsen, J.I., 2016. The last  
755 eurasian ice sheets - a chronological database and time-slice reconstruction, dated-1. *Boreas* 45, ~~44~~45–45.  
756 doi:10.1111/bor.12142.

757

758 Hughes, P.D., Gibbard, P.L., 2018. Global glacier dynamics during 100 ka pleistocene glaci  
759 ial cycles. *Quaternary Research (United States)* 90, 222–243. doi:10.1017/qua.2018.37.

760

761 Hughes, T., Denton, G.H., Grosswald, M., 1977. Was there a late-wiirm arctic ice sheet? *Nature* 266, 596–  
762 602. doi:<https://doi.org/10.1038/266596a0>.

763

764 Jakobsson, M., Nilsson, J., Anderson, L., Backman, J., Björk, G., Cronin, T.M., Kirchner, N., Koshurnikov,  
765 A., Mayer, L., Noormets, R., O'Regan, M., Stranne, C., Ananiev, R., Macho, N.B., Cherniykh, D., Coxall, H.,  
766 Eriksson, B., Floden, T., Gemery, L., Orjan Gustafsson, Jerraegan, M., Stranne, C., Ananiev, R., Macho, N.B.,  
767 Cherniykh, D., Coxall, H., Eriksson, B., Floden, T., Gemery, L., Orjan Gustafsson, Jerram m, K., Johansson, C.,  
768 Khortov, A., Mohammad, R., Semiletov, I., 2016. Evidence for an ice shelf covering the central arctic ocean  
769 during the penultimate glaciation. *Nature Communications* 7. doi:10.1038/ncomms10365.

770

- 771 Japsen, P., Green, P.F., Chalmers, J.A., Bonow, J.M., 2018. Mountains of southernmost norway: Uplifted  
772 miocene peneplains and re-exposed mesozoic surfaces. *Journal of the Geological Society* 175, ~~721-741~~721-  
773 741. doi:10.1144/jgs2017-157.
- 774
- 775 Jungclaus, J., Mikolajewicz, U., Kapsch, M.L., DiAgostino, R., Wieners, K.H., Giorgetta, M., Reick, C.,  
776 Esch, M., Bittner, M., Legutke, S., Schupfner, M., Wachsmann, F., Gayler, V., Haak, H., de Vrese, P.,  
777 Raddatz, T., Mauritsen, T., von Storch, J.S., Behrens, J., Brovkin, V., Claussen, M., Crueger, T., Fast, I.,  
778 Fiedler, S., Hagemann, S., Hohenegger, C., Jahns, T., Kloster, S., Kinne, S., Lasslop, G., Kornblueh, L.,  
779 Marotzke, J., Matei, D., Meraner, K., Modali, K., Mgemann, S., Hohenegger, C., Jahns, T., Kloster, S., Kinne,  
780 S., Lasslop, G., Kornblueh, L., Marotzke, J., Matei, D., Meraner, K., Modali, K., Müller, W., Nabel, J., Notz,  
781 D., Peters-von Gehlen, K., Pincus, R., Pohlmann, H., Pongratz, J., Rast, S., Schmidt, H., Schnur, R.,  
782 D., Peters-von Gehlen, K., Pincus, R., Pohlmann, H., Pongratz, J., Rast, S., Schmidt, H., Schnur, R.,  
783 Schulzweida, U., Six, K., Stevens, B., Voigt, A., Roeckner, E., 2019. Mpi-m mpi-esm1.2-lr model output  
784 prepared for cmip6 pmip lgm. URL: <https://doi.org/10.22033/ESGF/CMIP6.6642>,  
785 doi:10.22033/ESGF/CMIP6.6642
- 786
- 787 Kaplan, M. R., Hein, A. S., Hubbard, A. & Lax, S. M. Can glacial erosion limit the extent of glaciation?  
788 *Geomorphology* 103, 172–179 (2009).
- 789
- 790 Kessler, M.A., Anderson, R.S., Briner, J.P., 2008. Fjord insertion into continental margins driven by  
791 topographic steering of ice. *Nature Geoscience* 1, ~~365-369~~365-369. doi:10.1038/ngeo201.
- 792
- 793 Lamb, R.M., Harding, R., Huuse, M., Stewart, M., Brocklehurst, S.H., 2018. The early quaternary north sea  
794 basin. *Journal of the Geological Society* 175, ~~275-290~~275-290. doi:10.1144/jgs2017-057.
- 795
- 796 Liakka, J., Lofverstrom, M., Colleoni, F., 2016. The impact of the north american glacial topography on the  
797 evo- lution of the eurAsian ice sheet over the last glacial cycle. *Climate of the Past* 12, ~~1225-1241~~1225-1241.  
798 doi:10.5194/cp- 12-1225-2016.
- 799
- 800 Lidmar-Bergstrom, K., Ollier, C.D., Sulebak, J.R., 2000. Landforms and uplift history of southern norway.  
801 *Global and Planetary Change* 24, ~~211-231~~211-231. doi:10.1016/S0921-8181(00)00009-6.
- 802
- 803 Lindstrom, D.R., MacAyeal, D.R., 1986. Paleoclimatic constraints on the maintenance of possible ice-shelf  
804 cover in the Norwegian and Greenland seas. *Paleoceanography* 1, 313–337.  
805 doi:<https://doi.org/10.1029/PA001i003p00313>.
- 806
- 807 Lisiecki, L.E., Raymo, M.E., 2005. A pliocene-pleistocene stack of 57 globally distributed benthic  $\delta^{18}O$  records.  
808 *Paleoceanography* 20, ~~171-17~~171-17. doi:10.1029/2004PA001071.

809

810 Løseth, H., Nygard, A., Batchelor, C.L., Fayzullaev, T., 2022. A regionally consistent 3d seismic-stratigraphic  
811 framework and age model for the quaternary sediments of the northern north sea. *Marine and Petroleum*  
812 *Geology* 142, 105766. doi:10.1016/j.marpetgeo.2022.105766.

813

814 MacGregor, K.R., Anderson, R.S., Waddington, E.D., 2009. Numerical modeling of glacial erosion and  
815 headwall processes in alpine valleys. *Geomorphology* 103, ~~189~~189-204.  
816 doi:10.1016/j.geomorph.2008.04.022

817

818 Magrani, F., Valla, P.G., Egholm, D., 2022. Modelling alpine glacier geometry and subglacial erosion pat-  
819 terns in response to contrasting climatic forcing. *Earth Surface Processes and Landforms* 47, ~~1054~~1072-1054-  
820 1072.  
821 doi:10.1002/esp.5302.

822

823 Mas e Braga, M., Jones, R.S., Bernales, J. et al. A thicker Antarctic ice stream during the mid-Pliocene warm  
824 period. *Commun Earth Environ* 4, 321 (2023). <https://doi.org/10.1038/s43247-023-00983-3>

825

826 Millan, R., Mouginot, J., Rabatel, A., Morlighem, M., 2022. Ice velocity and thickness of the world's glaciers.  
827 *Nature Geoscience* 15, ~~124~~129-124-129. doi:10.1038/s41561-021-00885-z.

828

829 Millstein, J.D., Minchew, B.M., Pegler, S.S., 2022. Ice viscosity is more sensitive to stress than commonly  
830 assumed. *Communications Earth and Environment* 3. doi:10.1038/s43247-022-00385-x.

831

832 Nielsen, T., Mathiesen, A., Bryde-Auken, M., 2008. Base quaternary in the danish parts of the north sea and  
833 skagerrak. *Geological Survey of Denmark and Greenland Bulletin* , ~~37~~40doi:37-  
834 40doi:10.34194/geusb.v15.5038.

835

836 Olsen, L., Sveian, H., Ottesen, D., Rise, L., 2013. Quaternary glacial, interglacial and interstadial deposits of  
837 norway and adjacent onshore and offshore areas. *Geological Survey of Norway Special Publication* 13.

838

839 Patton, H., Hubbard, A., Andreassen, K., Winsborrow, M., Stroeven, A.P., 2016. The build-up, configuration,  
840 and dynamical sensitivity of the eurasian ice-sheet complex to late weichselian climatic and oceanic forcing.  
841 *Quaternary Science Reviews* 153, ~~97~~121-97-121.-URL: <http://dx.doi.org/10.1016/j.quascirev.2016.10.009>,  
842 doi:10.1016/j.quascirev.2016.10.009.

843

844 Patton, H., Hubbard, A., Heyman, J., Alexandropoulou, N., Lasabuda, A., Stroeven, A.P., 2022. The profound  
845 yet transient nature of glacial erosion , ~~1~~38doi:1-38doi:10.1038/s41467-022-35072-0.

846



847 [Paxman, G. J. G., Jamieson, S. S. R., Hochmuth, K., Gohl, K., Bentley, M. J., Leitchenkov, G., Ferraccioli, F.,](#)  
848 [2019. Reconstructions of Antarctic topography since the Eocene–Oligocene boundary. \*Palaeogeography,\*](#)  
849 [Palaeoclimatology, Palaeoecology, 535\(August\), 109346. <https://doi.org/10.1016/j.palaeo.2019.109346>](#)  
850

851 Pedersen, V.K., Huismans, R.S., Herman, F., Egholm, D.L., 2014. Controls of initial topography on temporal  
852 and spatial patterns of glacial erosion. *Geomorphology* 223, ~~96~~[11696-116](#). ~~URL:~~  
853 ~~<http://dx.doi.org/10.1016/j.geomorph.2014.06.028>~~, doi:10.1016/j.geomorph.2014.06.028  
854

855 Pedersen, V.K., Huismans, R.S., Moucha, R., 2016. Isostatic and dynamic support of high topography on a  
856 north atlantic passive margin. *Earth and Planetary Science Letters* 446, ~~1~~[91-9](#). ~~URL:~~  
857 ~~<http://dx.doi.org/10.1016/j.epsl.2016.04.019>~~, doi:10.1016/j.epsl.2016.04.019.  
858

859 Pedersen, V.K., Knutsen, Å. K., Pallisgaard-Olesen, G., Andersen, J.L., Moucha, R., Huismans, R.S., 2021.  
860 Widespread glacial erosion on the scandinavian passive margin. *Geology Early Publ*, ~~1~~[51-5](#).  
861 doi:10.1130/G48836.1/5304547/g48836.pdf.  
862

863 Pendergrass, A., Wang, J., National Center for Atmospheric Research Staff (Eds). Last modified 2022-11-07  
864 "The Climate Data Guide: GPCP (Monthly): Global Precipitation Climatology Project." Retrieved from  
865 <https://climatedataguide.ucar.edu/climate-data/gpcp-monthly-global-precipitation-climatology-project>  
866 on 2023-09-03.  
867

868 Rea, B.R., Newton, A.M.W., Lamb, R.M., Harding, R., Bigg, G.R., Rose, P., Spagnolo, M., Huuse, M., Cater,  
869 J.M.L., Archer, S., Buckley, F., Halliyeva, M., Huuse, J., Cornwell, D.G., Brocklehurst, S.H., Howell, J.A.,  
870 2018. Extensive marine-terminating ice sheets in europe from 2.5 million years ago. *Science Advances* 4,  
871 ~~eaar~~[8327](#). doi:10.1126/sciadv.aar8327.  
872

873 Rise, L., Ottesen, D., Berg, K., Lundin, E., 2005. Large-scale development of the mid-norwegian margin  
874 during the last 3 million years. *Marine and Petroleum Geology* 22, ~~33~~[4433-44](#).  
875 doi:10.1016/j.marpetgeo.2004.10.010.  
876

877 Sejrup, H.P., Clark, C.D., Hjelstuen, B.O., 2016. Rapid ice sheet retreat triggered by ice stream debuttressing:  
878 Evidence from the north sea. *Geology* 44, ~~355~~[358355-358](#). doi:10.1130/G37652.1.  
879

880 Sejrup, H.P., Landvik, J.Y., Larsen, E., Janockom, J., Eiriksson, J., King, E., 1998. The jf fren area, a border  
881 zone of the norwegian channel ice stream.  
882

883 Sejrup, H.P., Larsen, E., Haflidason, H., Berstad, I.M., Hjelstuen, B.O., Jonsdottir, H.E., King, E.L., Landvik,  
884 J., Longva, O., Nygard, A., Ottesen, D., Raunholm, S., Rise, L., Stalsberg, K., 2003. Configuration, history  
885 and impact of the norwegian channel ice stream. *Boreas* 32, ~~183~~18-36. doi:10.1080/03009480310001029.  
886

887 Simms, A.R., Lisiecki, L., Gebbie, G., Whitehouse, P.L., Clark, J.F., 2019. Balancing the last glacial maximum  
888 (lgm) sea-level budget. *Quaternary Science Reviews* 205, ~~143~~143-153.  
889 doi:10.1016/j.quascirev.2018.12.018.  
890

891 Steer, P., Huismans, R.S., Valla, P.G., Gac, S., Herman, F., 2012. Recent glacial erosion of fjords and low-  
892 relief surfaces in western scandinavia. *Nature Geoscience* 14, 4433. URL: <http://dx.doi.org/10.1038/ngeo1549>,  
893 doi:<http://www.nature.com/ngeo/journal/v5/n9/abs/ngeo1549.htmlsupplementary-information>.  
894

895 [Stroeven, A. P., Hättestrand, C., Kleman, J., Heyman, J., Fabel, D., Fredin, O., Goodfellow, B. W., Harbor, J.](#)  
896 [M., Jansen, J. D., Olsen, L., Caffee, M. W., Fink, D., Lundqvist, J., Rosqvist, G. C., Strömberg, B., & Jansson,](#)  
897 [K. N. \(2016\). Deglaciation of Fennoscandia. \*Quaternary Science Reviews\*.](#)  
898 <https://doi.org/10.1016/j.quascirev.2015.09.016>  
899

900 Wickert, A. D. (2016), Open-source modular solutions for flexural isostasy: gFlex v1.0, *Geosci. Model Dev.*,  
901 9(3), ~~997~~997-1017, doi:10.5194/gmd-9-997-2016.  
902

903 [Zeitz, M., Levermann, A., and Winkelmann, R.: Sensitivity of ice loss to uncertainty in flow law parameters](#)  
904 [in an idealized one-dimensional geometry, \*The Cryosphere\*, 14, 3537–3550, \[https://doi.org/10.5194/tc-14-\]\(https://doi.org/10.5194/tc-14-3537-2020\)](#)  
905 [3537-2020, 2020.](#)